Numerical modeling of pressure drops in micro-channels with various pillars arrangements: squared and staggered.

Jalil Ouazzani – **ArcoFluid** (Bordeaux, France)
Yves Garrabos, Romain Guillaument, Carole Lecoutre, Samuel Marre & Sandy Morais – **ICMCB** (Pessac, France).

High-pressure micro-models are very useful tools to directly visualize the pore-scale fluid distribution and displacement, by injecting for example CO_2 into a water-saturated micro porous media at the geological reservoir conditions. ICMCB researchers have performed fluid flow experiments performed within a well-designed two-dimensional pore network inside the high-pressure silicon/Pyrex micro-models. Obviously, such micro-models have a low pertinence with respect to the local complexity encountered in the 3D porous media of the geological formations and the measurements of the local velocity field always remain a non-resolved challenging problem, especially at high pressure and high temperature. However, they can take advantage of their 2D characteristics to observe, for the first time in real p,T conditions, the behavior of the two-phase distribution at different operating conditions. The combination between flow rate and pressure measurements, wettability change of the solid walls, and the video recording of the pore network, can be then used to capture some of the key mechanisms at a typical pore scale of a few tens of micrometers. Besides the experiments, numerical modeling of such experiments has been done using the PHOENICS software from CHAM LTD. First to validate the numerical model which will be used at ICMCB, it has been tested against a thorough published experiments of water injection in micro-model at various Reynolds number, and plots arrangements (Measurement of pressure drop and flow resistance in micro-channels with integrated micro-pillars: Microfluid Nanofluid (2013) 14:711–721 - DOI 10.1007/s10404-012-1089-1.

Using the PHOENICS code, we started with 2D models but found out that the pressure drop was way off from the one obtained through experiments. This is mainly due to the short height of channel which makes friction from top and bottom walls a substantial effect. Therefore we resorted to a full three dimensional calculations. These calculations are costly due the large amounts of pillars in the channel. These 3D computational models reproduced satisfactorily the expected pressure drop. However due to the small height of the rectangular channels used in these study, we have investigated the 2D-Helle-Shaw formulation and found a very good agreements with the 3D models with a much lower CPU cost.

Description of Physical problem

In this study, the authors investigate single phase fluid flow through micro-channels with integrated micro-pillars to calculate pressure drop and flow resistance. The micro-channels, which contain micro-pillars arranged in a square and staggered arrangement, are fabricated in silicon substrate. The microfluidic devices were designed to cover a range of different pillar diameter and porosity. Dimensions of some of the fabricated samples chosen for modeling are listed in Table 1 and shown in Fig. 1. In Table 1, d is cylindrical pillars diameter, S is distance between pillars, W is the width of the micro-channel, h is the depth of the channel or height of the pillar, L is the distance occupied by pillars, NSq is the notation for square arrangement and NSt is the notation for staggered arrangement. For example, the arrangement NSq-50-100 corresponds to a square configuration of pillars with a pillar diameter of 100 mm and porosity of 50%.

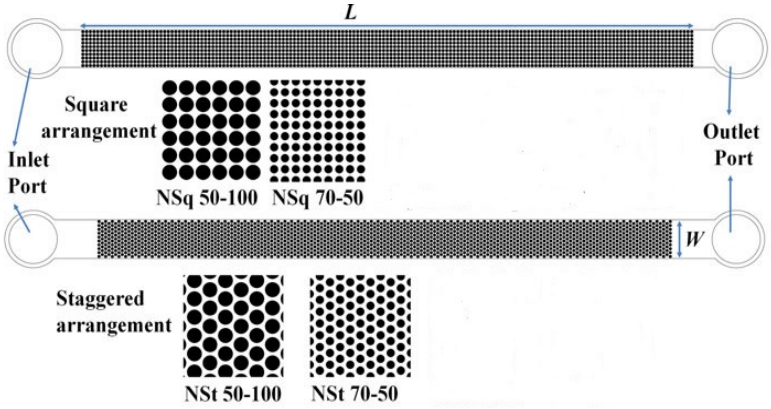

Fig. 1 Micro-channel with integrated micro-pillars (MCIP) considered in this work. NSq refers to square arrangement and NSt refers to staggered arrangement.

Arrangement	Pillar	Dimensions	Channels	Dimensions

	d (mm) Diameter	S (mm) Distance between pillars	h (mm) height of channel	L (mm) Length of channel	W (mm) Width of channel
Nsq 70-50	50.2	82	98.4	24.46	808
Nsq 50-100	100	124	98.4	18.87	1250
Nst 70-50	50	87.2	98.4	24.26	869
Nst 50-100	100	135	98.4	20.11	1346

Table 1: Geometrical dimensions of different fabricated MCIPs considered in the present work. Hereafter the disposition for S and d for squared and staggered configurations.

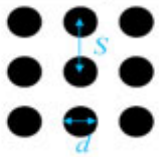

Square

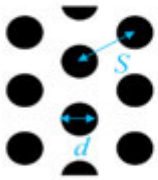

Staggered

Mathematical Model

For such problem of pressure drops in channels, a useful non dimensional number to introduce is the Reynolds number: $\mathrm{Re} = \frac{\rho_{ref} U_{ref} L_{ref}}{\mu_{ref}}$ where all the parameters with ref subscript denotes reference values defined in the following.

So we will make the steady Navier-Stokes equations non dimensional by using the following reference values:
L_{ref} = d (diameter of pillar (m)), U_{ref}= U_0 (Inlet Velocity (m/s)), t_{ref} (time = L_{ref}/U_{ref} (s)), r_{ref} (Standard density of water = 998 .22998 (Kg/m^3)), m_{ref} (Dynamic viscosity of water = 1.0042 10^{-3} (Pa.s)), P_{ref} (Reference Pressure = $r_{ref}*U_{ref}^2$ (Pa)).

The non-dimensional equations become:

$$\vec{V}\nabla\vec{V} = -\nabla p + \frac{1}{\mathrm{Re}}\Delta\vec{V} + F_{HS} \quad (1)$$

$$\nabla\cdot\vec{V} = 0 \quad (2)$$

The term FHS is added for the 2D Hele Shaw approximation, otherwise this term is zero.

$$F_{HS} = -\frac{12}{\varepsilon\,\mathrm{Re}\,h_*^2}\vec{V} \quad (3)$$

Where e is porosity, $h_* = \frac{h}{d}$ non-dimensional height of the channel.

The 2D-Helle-Shaw formulation is accurate under the condition that the channel depth h is small compared to its width w which is the case here (H. Bruus. Theoretical microfluidics. Oxford
Master Series in Condensed Matter Physics, 2008).

Results and discussion

In the numerical model we will show successively the results from the 2D approach, then with the full 3D model and we give the alternative of the 2D Hele Shaw model. In order to have accurate results, we have to construct an identical model to the experimental one and then have enough mesh size in all spatial directions. In all these cases we have used 436 x 50 x 12, in the X (axial direction), Y (transverse direction) & Z (depth direction) directions respectively. In the transverse direction, only half of the domain used through symmetry.

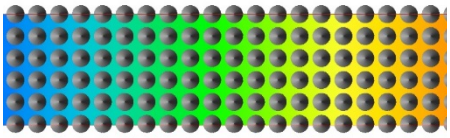

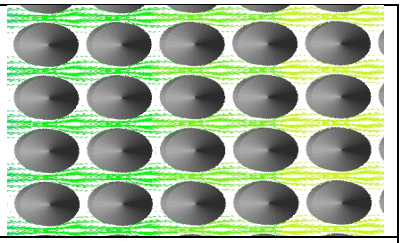

Square arrangement Nsq 50-100

Vector fields for Nsq 50-100

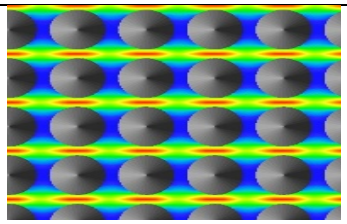

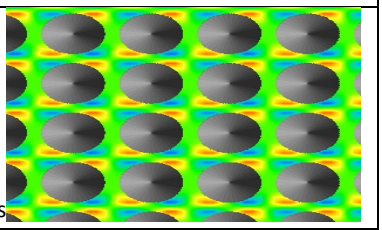

Axial Velocity contours for Nsq 50-100

Transverse velocity contours for Nsq 50-100

Figure 2: View of the square arrangement for Nsq 50-100 and vectors and velocity field's contours

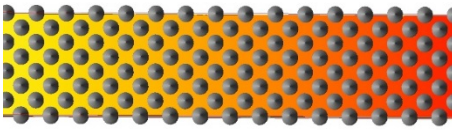

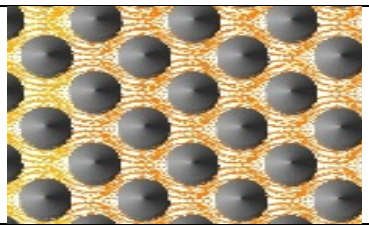

Square arrangement Nst 50-100

Vector fields for Nst 50-100

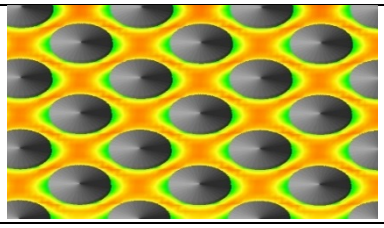

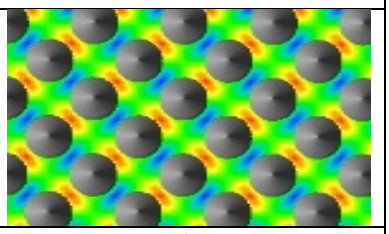

Axial Velocity contours for Nst 50-100

Transverse velocity contours for Nst 50-100

Figure 3: View of the staggered arrangement Nst 50-100 and vectors and velocity field's contours

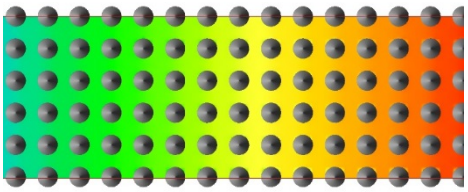

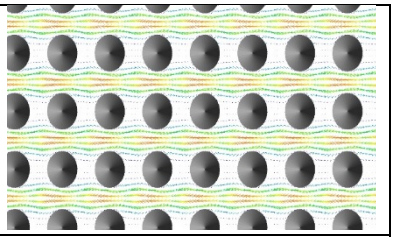

Square arrangement Nsq 70-50

Vector fields for Nsq 70-50

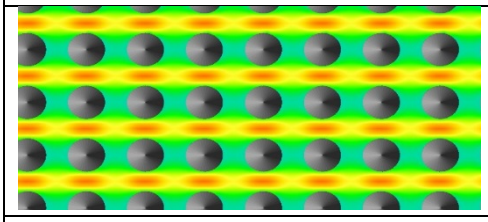

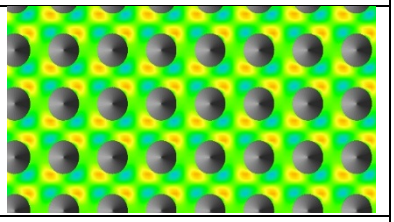

Axial Velocity contours for Nsq 70-50

Transverse velocity contours for Nsq 70-50

Figure 4: View of the squared arrangement Nsq 70-50 and vectors and velocity field's contours

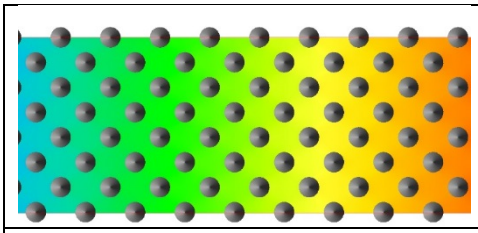

Square arrangement Nst 70-50

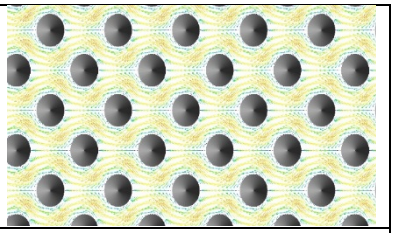

Vector fields for Nst 70-50

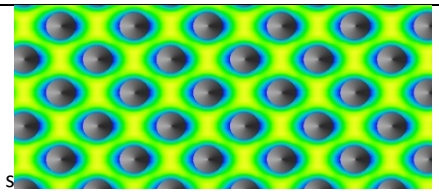

Axial Velocity contours
for Nst 70-50

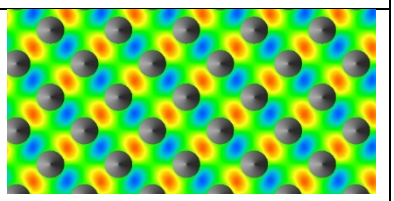

Transverse velocity contours
for Nst 70-50

Figure 5: View of the staggered arrangement Nst 70-50 and vectors and velocity field's contours

Comparing the results from squared and staggered we can see that the squared cases have higher pressure drop than their equivalent in the staggered case. This can be explained rom the fact that in the squared case the flow goes straight and exerts force to itself leaving large amount of empty space whereas in the staggered the flow occupy the full domain. When analyzing table 2 and figures 6-9, we can see that the pressure drop from the 2D cases are always much lower than the experimental values and in order to correct the nascence of friction due to the top and low walls of the channels we have to resort to the full 3D model which gives us very close results in the staggered cases and close results in the squared cases (uncertainty in the spacing of pillars can lead to a large discrepancies in the final pressure drop results). It is quite clear that to determine permeability correlations from 2D results will be inaccurate (this will be more pronounced when depth of channel is even smaller).

Therefore using the Hele Shaw alternative for narrow depth channels is a quite good option to be able to compute in 2D but to account for the friction of top and bottom walls through an inertial source term. The results from the Hele Shaw model are in some cases identical to the results from the 3D model as can be seen in figure 6 to 9. The source term equation (3) which appears in equation (1) is introduced in PHOENICS through user coding (INFORM).

Conclusion

The modeling of flow through pillars in micro channels has been done for several rectangular channels with various pillars arrangement (squared and staggered) using the PHOENICS code from CHAM ltd. The 3D results compare favorably to the experiments but not the 2D results. It has been show that using for such channels (depth/width small) the Hele Shaw formulation, gives the same results as the 3D cases but using a modified 2D approach. The next work will be to combine the Darcy and the Hele Shaw approach.

NST 70-50	Q=50ml/min	Q=100ml/min	Q=200ml/min
2D	0.989 10^5 Pa.m^{-1}	1.98 10^5 Pa.m^{-1}	3.99 10^5 Pa.m^{-1}
2D Hele Shaw	1.35 10^5 Pa.m^{-1}	2.7 10^5 Pa.m^{-1}	5.41 10^5 Pa.m^{-1}
3D	1.45 10^5 Pa.m^{-1}	2.88 10^5 Pa.m^{-1}	5.82 10^5 Pa.m^{-1}
Experiments	1.40 10^5 Pa.m^{-1}	2.78 10^5 Pa.m^{-1}	5.80 10^5 Pa.m^{-1}

(a)

NST 50-100	Q=50ml/min	Q=100ml/min	Q=200ml/min
2D	1.09 10^5 Pa.m^{-1}	2.18 10^5 Pa.m^{-1}	4.39 10^5 Pa.m^{-1}
2D Hele Shaw	1.55 10^5 Pa.m^{-1}	3.1 10^5 Pa.m^{-1}	6.23 10^5 Pa.m^{-1}
3D	1.54 10^5 Pa.m^{-1}	3.1 10^5 Pa.m^{-1}	6.25 10^5 Pa.m^{-1}
Experiments	1.50 10^5 Pa.m^{-1}	3.0 10^5 Pa.m^{-1}	6.20 10^5 Pa.m^{-1}

(b)

NSQ 70-50	Q=50ml/min	Q=100ml/min	Q=200ml/min
2D	1.75 10^5 Pa.m^{-1}	3.5 10^5 Pa.m^{-1}	7.03 10^5 Pa.m^{-1}
2D Hele Shaw	2.18 10^5 Pa.m^{-1}	4.36 10^5 Pa.m^{-1}	9 10^5 Pa.m^{-1}
3D	2.19 10^5 Pa.m^{-1}	4.31 10^5 Pa.m^{-1}	9.02 10^5 Pa.m^{-1}
Experiments	2.3 10^5 Pa.m^{-1}	4.8 10^5 Pa.m^{-1}	9.95 10^5 Pa.m^{-1}

(c)

NSQ 50-100	Q=50ml/min	Q=100ml/min	Q=200ml/min
2D	2.2 10^5 Pa.m^{-1}	4.6 10^5 Pa.m^{-1}	9.2 10^5 Pa.m^{-1}
2D Hele Shaw	2.94 10^5 Pa.m^{-1}	5.89 10^5 Pa.m^{-1}	11.79 10^5 Pa.m^{-1}
3D	2.93 10^5 Pa.m^{-1}	5.92 10^5 Pa.m^{-1}	11.95 10^5 Pa.m^{-1}
Experiments	3.0 10^5 Pa.m^{-1}	6.3 10^5 Pa.m^{-1}	12.75 10^5 Pa.m^{-1}

(d)

Table 2: Pressure drop results summary for all cases and models:
(a) Nst 70-50 (b) Nst 50-100 (c) Nsq 70-50 (d) Nsq 50-100.

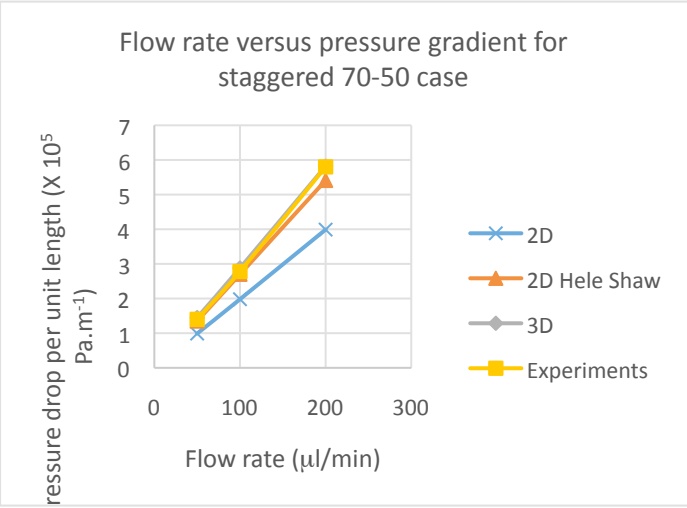

Figure 6: Variation of pressure drop with change in flow rate for 2D, 2D-HS, 3D and NST 70-50 experiments.

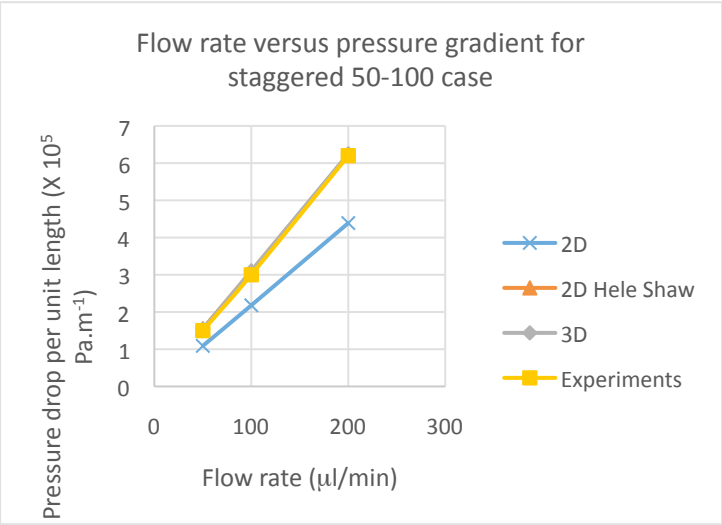

Figure 7: Variation of pressure drop with change in flow rate for 2D, 2D-HS, 3D and NST 50-100 experiments.

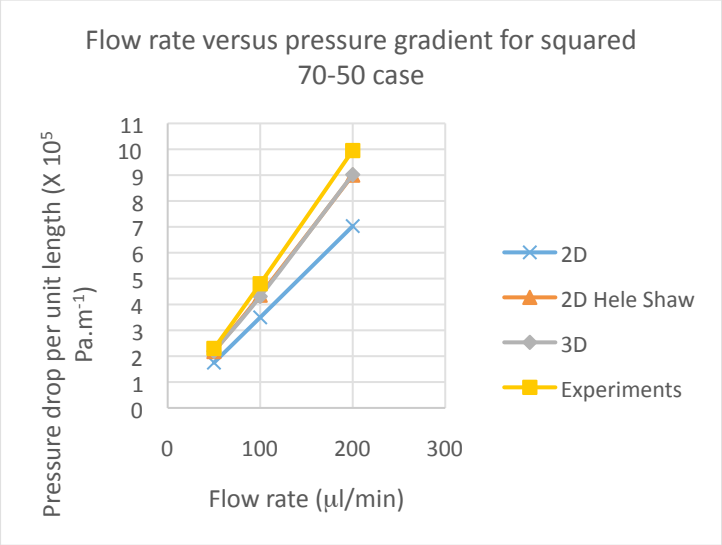

Figure 8: Variation of pressure drop with change in flow rate for 2D, 2D-HS, 3D and NSQ 70-50 experiments.

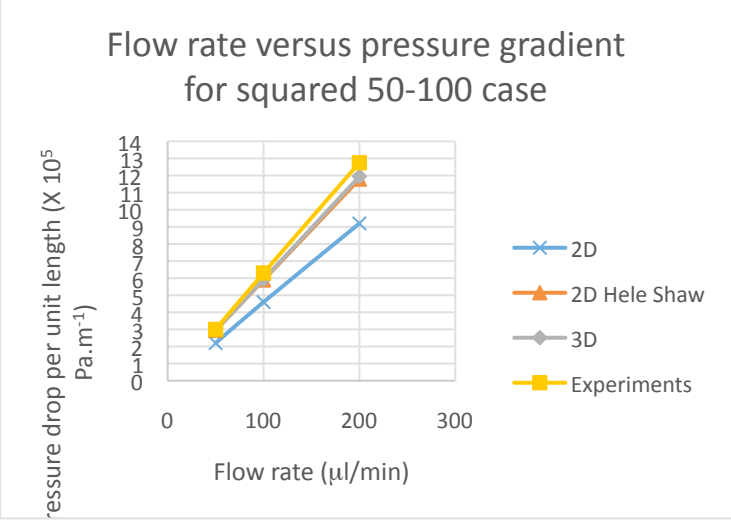

Figure 9: Variation of pressure drop with change in flow rate for 2D, 2D-HS, 3D and NSQ 50-100 experiments.